Du et al. AMB Expr (2016) 6:81
DOI 10.1186/s13568-016-0257-1

AMB Express

ORIGINAL ARTICLE

Open Access

Identifying the role of reactive oxygen species (ROSs) in *Fusarium solani* spores inactivation

Yilin Du[1], Houfeng Xiong[1], Shuangshi Dong[1*], Jun Zhang[1], Dongmei Ma[1] and Dandan Zhou[2,3*]

Abstract

The inactivation mechanism of photocatalytic disinfectants on bacteria is well known. In contrast, the potential inactivation of fungal spores by visible-light induced photocatalysis has been recognized, but the inactivation mechanism is poorly understood. We hypothesize that photocatalytically generated reactive oxygen species (ROSs) are directly involved in this mechanism. To test this hypothesis, we identified the roles of ROSs in the inactivation of *Fusarium solani* spores. As the photocatalysts, we doped TiO_2 with 3 typical dopants, forming Ag/TiO_2, N/TiO_2 and Er^{3+}:$YAlO_3$/TiO_2. The Ag/TiO_2 photocatalysis was dominated by H_2O_2, with the longest lifetime among the investigated ROSs. Ag/TiO_2 photocatalysis yielded almost 100 % inactivation efficiency and preserved the cell-wall shape of the spores, thus minimizing the biomolecule leakage. Er^{3+}:$YAlO_3$/TiO_2 was dominated by h^+ ROSs, yielding an inactivation efficiency of 91 %; however, the severe leakage released large numbers of molecular bio-products. Severe damage to the cell walls by the h^+ species was confirmed in micrograph observations. Subsequent to cell wall breakage, the Er^{3+}:$YAlO_3$/TiO_2 nanoparticles entered the spore cells and directly oxidized the intracellular material. The N/TiO_2 photocatalysis, with $\bullet O_2^-$ dominated ROSs, delivered intermediate performance. In conclusion, photocatalysts that generate H_2O_2-dominated ROSs are most preferred for spore inactivation.

Keywords: *F. solani*, Visible light, Photocatalysis, Inactivation, Soluble microbial products, Spore

Introduction

According to the Food and Agriculture Organization of the United Nations, agriculture is the largest consumer of fresh water (Polo-López et al. 2014). Therefore, the reuse of wastewater for agriculture irrigation has received much attention in recent years. However, wastewater contains various pathogens that must be removed before the irrigation. Among these pathogens are phytopathogenic fungi such as *Fusarium*, *Pythium*, *Phytophthora* and *Olpidium* species. The *Fusarium* genus, which is widely distributed in water and soil systems, causes decay of roots, stems and flowers. *Fusarium* spores, which develop into *Fusarium* fungal cells, are very difficult to inactivate owing to their thick cell walls and strong environmental resistance (Polo-López et al. 2010).

One of the most promising methods for disinfecting *Fusarium* spores is photocatalytic inactivation (Fernández-Ibáñez et al. 2009). The photocatalytic inactivation should preferably be mediated by visible light, because UV light comprises only 5 % of the solar light (Zuo et al. 2012). Moreover, the photocatalytic performances of *Fusarium* spore disinfection are affected by the properties of the photocatalysts, such as the adsorption capability of the nanoparticles on the spores (Polo-López et al. 2010), and the morphology (nanotubes, nanoplates, nanorods or nanospheres) (Turki et al. 2013) and components (Fernández-Ibáñez et al. 2015) of the photocatalysts.

In essence, the inactivation capability of a photocatalyst depends on the reactive oxygen species (ROSs) it can generate. As photocatalysts adsorb irradiation with

*Correspondence: dongshuangshi@gmail.com; zhoudandan415@163.com
[1] Key Laboratory of Groundwater Resources and Environment, Ministry of Education, Jilin University, Changchun 130021, Jilin, China
[2] School of Environment, Northeast Normal University, Changchun 130117, China
Full list of author information is available at the end of the article

energies equal to or greater than their band gap energies, they generate e^-/h^+ pairs (Hou et al. 2012). In aqueous environments, ROSs are released through the chemical reaction of photogenerated species on TiO_2 surfaces (Thabet et al. 2013). The released ROSs, which include e^-, h^+, •OH, H_2O_2, and $•O_2^-$, then disinfect the fungal spores (Xia et al. 2013). The significant role of ROSs in phototocatalytic bacterial disinfection is well recognized (Foster et al. 2011). The inactivation efficiency against *Escherichia coli* is linearly related to the steady-state •OH concentration, suggesting that •OH is the predominant inactivation species in this organism (Cho et al. 2005). This conclusion was disputed by Kikuchi et al. (1997), who separated *E. coli* suspension from a TiO_2 thin film through hydrophilic polytetrafluoroethylene membranes. They found that neither the half-life nor the half diffusion length of •OH was sufficient to traverse the membrane and inhibit the *E. coli* cells. Therefore, they concluded that the major bactericidal species was H_2O_2 rather than •OH. ROSs can also attack the cell walls, causing leakage of intracellular macromolecules such as proteins and nucleic acids from the cells (Rahmanto et al. 2005). The leaking biomolecules can lower the efficiency of the treatment and adversely affect the effluent quality, seriously compromising the health of the receiving waters (Xie et al. 2012). Consequently, when applying a photocatalytic disinfection, we must also monitor the subsequent increment in soluble microbial products (SMPs).

The effects of ROSs on the disinfection efficiency and SMP release are well known in bacterial disinfection, but are poorly understood in fungal spore disinfection. In visible light photocatalysis, modifying the TiO_2 surface with different dopants will alter the generated ROSs (Chong et al. 2014). The diverse TiO_2 crystal structure admits a variety of dopants (Shah et al. 2002), inducing different spore-inactivation mechanisms. Among the versatile dopants trialed in recent studies, the most effective were the metallic element Ag (Lee et al. 2005), the nonmetal element N (Nakamura et al. 2004) and the upconversion luminescence agent Er^{3+}:$YAlO_3$ (Zhou et al. 2015). Under visible light, the silver atoms in Ag/TiO_2 play a co-catalytic role by injecting plasmon-induced electrons into the photocatalyst. Thus, TiO_2 generates high e^-/h^+ pair separation under visible light (Lee et al. 2005). In contrast, the nitrogen-doped TiO_2 can respond to visible light because the N atoms decrease the band energy gap (Lu et al. 2014). In Er^{3+}:$YAlO_3/TiO_2$, the photocatalytic material assembles with the upconversion luminescence agents Er^{3+}:$YAlO_3$ (Wang et al. 2010), transforming the visible light to UV light and thus satisfying the requirement for anatase TiO_2 photocatalysis (Dong et al. 2015).

In summary, photocatalytic inactivation of fungal spores is worthy of consideration, but the activation mechanism remains to be elucidated. In this work, we prepared three kinds of photocatalysts; a metal-doped photocatalyst (Ag/TiO_2), a nonmetal-doped photocatalyst (N/TiO_2) and an upconversion luminescence agent-doped photocatalyst (Er^{3+}:$YAlO_3/TiO_2$), which were expected to generate different ROSs. We investigated the ability of the three photocatalysts to inactivate *Fusarium solani* (*F. solani*) spores, and the subsequently retained inactivation by-products. By analyzing the dominant ROSs released by the photocatalysts, we identified the preliminary mechanisms of photocatalytic spore inactivation, and highlighted the need for appropriate photocatalysts selection in future.

Materials and methods

Catalyst preparation

Nano-sized Ag/TiO_2 particles were prepared by a sol–gel process as described in Lee et al. (2005). The nitrogen-doped photocatalysts were prepared by the calcinations method, using urea as the nitrogen source (Kontos et al. 2008). The Er^{3+}:$YAlO_3/TiO_2$ was prepared by a sol–gel method described in Dong et al. (2015).

Fungal strain, cultivation and enumeration

Fusarium solani was purchased from Beina Chuanglian Biotechnology Institute. (Beijing, China, No. BNCC144579). Colonies of *F. solani* were transferred to sporulation agar medium containing potassium chloride and kept at 25 °C for 15 days (Fernández-Ibáñez et al. 2009). The spores were washed from the medium using sterilized distilled water. The obtained mixed suspension was centrifuged at 300×*g* for 10 min and washed three times with sterilized distilled water. The concentration of the suspension was determined by direct count in a counting chamber (Turki et al. 2013). The initial experimental concentration was approximately 10^4 CFU/mL. The fungal spore concentration during photocatalysis was determined by the pour plate technique (i.e., by spreading 100 μL of the sample in the plate, and counting the resulting colonies) (Polo-López et al. 2014). All samples and treatments were prepared in triplicate and the plates were incubated at 28 °C for 2 days in the dark before counting (Polo-López et al. 2014).

Photocatalytic inactivation

The experiments were performed in 27.5-mm × 95-mm (diameter × height) sealed glass bottles with a working volume of 40 mL. The light source was a 300-W xenon lamp with a 420-nm cutoff and an intensity of ~100 mW/cm^2. The light beam was horizontally projected on the side wall of the bottle. In a typical inactivation test, the bottles containing magnetic stirrers were pre-sterilized before each batch.

The *F. solani* spores (initial concentration ~ 10^4 CFU/mL) and photocatalyst powder (1 g/L) were then added to the sterilized bottles. All experiments were performed in triplicate at room temperature (~20 °C).

The scavenging species and their concentrations in the scavenging experiments were as follows: 0.5 mmol/L sodium oxalate, 0.5 mmol/L isopropanol, 0.05 mmol/L Cr(VI), 0.1 mmol/L Fe(II)-EDTA, and 2 mmol/L TEMPOL. By quenching the specific reactive species with individual scavengers, we can specify the reactive species' contributions in the different photocatalytic systems: Cr(VI) for e^-, isopropanol for •OH, sodium oxalate for h^+, Fe(II) for H_2O_2, and TEMPOL for $\bullet O_2^-$ (Xia et al. 2013).

Analytical methods

X-ray diffraction (XRD) analysis

Powder XRD patterns were acquired by a Bruker D8 Advanced X-ray diffractometer using Cu Kα radiation (λ = 0.15418 nm) at a scanning rate of 2°/min. The 2θ range was 10°–90°.

Optical microscope

Drop samples were collected from the reaction solution at 0 and 4 h. The samples were observed under an optical microscope (CKX41, Olympus).

Transmission electron microscopy (TEM)

Samples (10 mL) were collected from the reaction solutions at 0 and 4 h, centrifuged and washed three times with 0.1 M phosphate buffer (PBS, pH = 7.2). Cell pellets of the samples were prepared by pre-fixing in 2.5 % glutaraldehyde at 4 °C for 12 h, washing three times with PBS, then pre-fixing in 1 % osmium tetroxide at 4 °C for 3 h. The cell pellets were dehydrated through a series of ethanol with graded concentration and embedded in Spurr solution at 70 °C for polymerization. The polymerized samples were sectioned into ultrathin slices (70 nm) using an ultramicrotome (Leica, Reichert Ultracuts, Wien, Austria), and stained with uranyl acetate and lead citrate. Finally, the sections were observed in a JEM1230 transmission electron microscope (JEOL Ltd., Tokyo, Japan).

Three-dimensional fluorescence spectra (EEM) measurements

The reaction solution (10 mL) was sampled from the three photocatalyst preparations at 0, 1 and 7 h, then filtered through a 0.22-μm membrane to remove the fungal cells. EEM spectroscopy measurements were conducted using a fluorescence spectrometer (F-7000, Hitachi, Japan) at a scan rate of 2000 nm/min and an excitation/emission slit bandwidth of 5 nm. The scanning field was set to 220–600 nm for the emission spectra and 220–450 nm for the excitation spectra.

Molecular weight (MW) analysis

The molecular weight of the aqueous phase was analyzed by gel filtration chromatography (GFC, Shimadzu, Japan), which performs high performance liquid chromatography (LC-10A, Shimadzu, Japan) with a differential refractive index (RID-10A, Shimadzu, Japan) detector. As the standard, we used glucan, which covers a molecular weight range of 200–1500,000 Da. The column temperature was controlled at 40 °C. The mobile phase was deionized doubly distilled water with a flow rate of 0.6 mL/min, and the hydraulic detention time of the column was 30 min.

Results

Characterization of the prepared photocatalysts

Figure 1 shows the XRD spectra of the prepared N/TiO_2, Er^{3+}:$YAlO_3$/TiO_2 and Ag/TiO_2 photocatalysts. The peaks in the XRD spectra of the three photocatalysts are generally sharp, with small full-width-at-half maximums. Therefore, the formation of the crystals was basically complete, and the photocatalysts were receptive to the photocatalytic reaction. The doping mechanisms of these nanoparticles were described above.

The three photocatalysts presented different characteristics as they were doped with different materials. The phase structure of the prepared Ag/TiO_2 was pure anatase TiO_2. The N/TiO_2 nanoparticles exhibited a phase structure of mixed anatase and rutile with mass fractions of ~97 and 3 %, respectively (computed by the Spurr–Myers equation; Spurr and Myers 1957). Er^{3+}:$YAlO_3$/TiO_2 presented two crystal forms; the visible light up-conversion components Er^{3+}:$YAlO_3$ and anatase, indicating that Er^{3+}:$YAlO_3$ was successively doped in the anatase TiO_2 (Dong et al. 2015).

Inactivation of *F. solani* spore by the prepared photocatalysts

Figure 2 compares the *F. solani* spore counts during photocatalysis inactivation with the three prepared photocatalysts under visible light irradiation. All of the photocatalysts efficiently inactivated the spores. Over a 4-h period, N/TiO_2 and Er^{3+}:$YAlO_3$/TiO_2 (at dosages of 1 g nanoparticles/L) achieved inactivation efficiencies of 78 and 87 %, respectively. During the following 3 h, the removal rates of living cells continuously increased, reaching 91 and 94.3 %, respectively. Notably, the Ag/TiO_2 nanoparticles inactivated 99.5 % of the *F. solani* cells within 1 h of irradiation, and nearly all cells were inactivated within 4 h. Obviously, Ag/TiO_2 demonstrated higher fungal infection capability than the other photocatalysts. In comparison, none of the control treatments—visible light photolysis alone (no catalysts), dark adsorption (no irradiation) and the blank control (neither

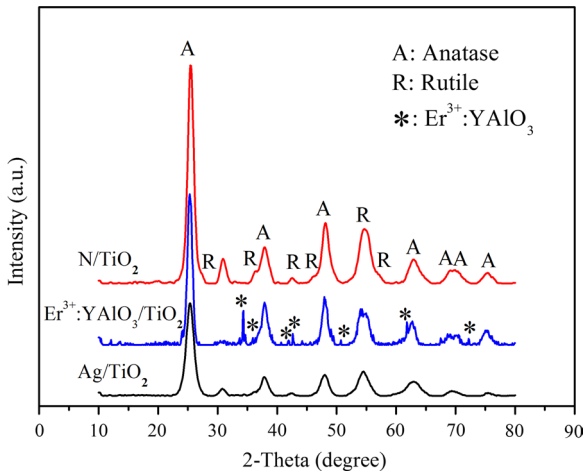

Fig. 1 XRD spectra of the prepared photocatalysts

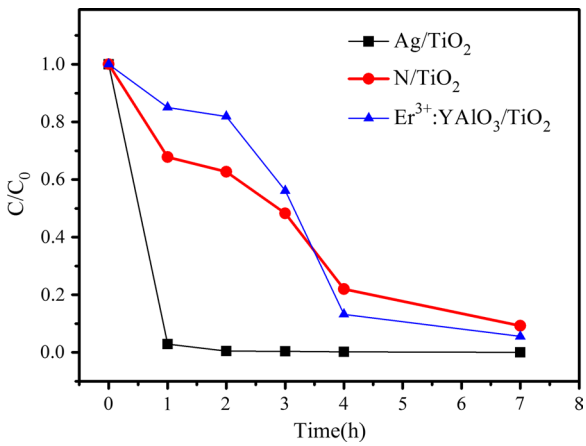

Fig. 2 Inactivation of *F. solani* using Ag/TiO_2, N/TiO_2 and Er^{3+}:$YAlO_3$/TiO_2photocatalysts under visible light irradiation. All the values are obtained based on the average of three times experiments

catalysts nor irradiation)—noticeably inactivated the *F. solani* spores (data not shown).

Micro-observation of the inactivated spores

To better understand the inactivation mechanism, the outer shape and inner-microstructures of *F. solani* before and after photocatalysis were examined under an optical microscope and TEM, respectively. As shown in Fig. 3, the active *F. solani* spore cells were sickle-shaped, with approximate lengths of 10 μm and cell-wall thicknesses of 0.3 μm. Regular cell walls, membranes, nuclei and mitochondria-like components were clearly visible inside the cells.

All of the inactivation protocols shrunk the cells, deformed their shapes, and generated large quantities of cell debris. The photocatalyst nanoparticles were obviously adsorbed on the cell surfaces, causing initial physical damage to the cells (Caballero et al. 2009). The Ag/TiO_2 photocatalysis, which performed most efficiently among the three treatments, exhibited the highest number of photocatalysts enclosing the spores. Such direct contact suggests direct oxidation of the cell components and high killing efficiency against the microorganisms (Rahmanto et al. 2005), and is especially significant for *F. solani* spores with their relatively thick cell walls (Thabet et al. 2014). Interestingly, the Er^{3+}:$YAlO_3/TiO_2$ protocol performed less efficiently than Ag/TiO_2, but caused much greater spore damage and produced the most cell debris among the protocols. These various consequences were related to the different ROSs characteristics of the photocatalysts.

The TEM results revealed microscopic changes in the spore cells (Fig. 3). After 4 h photocatalysis by all three protocols, the cells were disrupted to various degrees, showing damage features such as plasmolysis and ghosting of the intracellular vacuoles. Most of the intracellular components became unclear, indicating their decay. The Ag/TiO_2 protocol best preserved the cell wall structure, but cytoplasm leaking was observed. The N/TiO_2 protocol partially oxidized the cell wall, releasing the spore cell contents; further photocatalytic oxidization should completely kill the spores. No nanoparticles were observed in the spore cells subjected to these two protocols. In contrast, the Er^{3+}:$YAlO_3/TiO_2$ photocatalysis introduced some nanoparticles into the inactivated spores (indicated by the red arrow). In these spore cells, the cytoplasm was seriously disrupted and even partially disappeared. The Er^{3+}:$YAlO_3/TiO_2$ treatment yielded the thinnest cell walls among the three protocols, suggesting the strongest attacking capability on the spore cell wall, despite its weaker inactivation capability than Ag/TiO_2 (see Fig. 2).

Biomolecules leakage and degradation during inactivation

The EEM spectrum provides clues into the subsequent SMP release during the photocatalytic inactivation. Figure 4 shows the main SMP constituents in the spore cells prior to inactivation. We observe tyrosine/tryptophan amino acids (in region I), soluble microbial byproduct-like materials (in region VI) and humic acid-like organics (in region V). As evidenced by the gradual weakening of their peaks, all of these SMP constituents were significantly reduced by the Ag/TiO_2 and N/TiO_2 photocatalysts. Again, the Ag/TiO_2 photocatalysis demonstrated much higher removal efficiency for the generated SMPs than the other protocols. The tyrosine/tryptophan amino acid and soluble microbial byproduct-like compounds were almost completely removed, and the humic acid-like compounds were dramatically decreased. It appears that the Ag/TiO_2 and N/TiO_2 treatments simultaneously

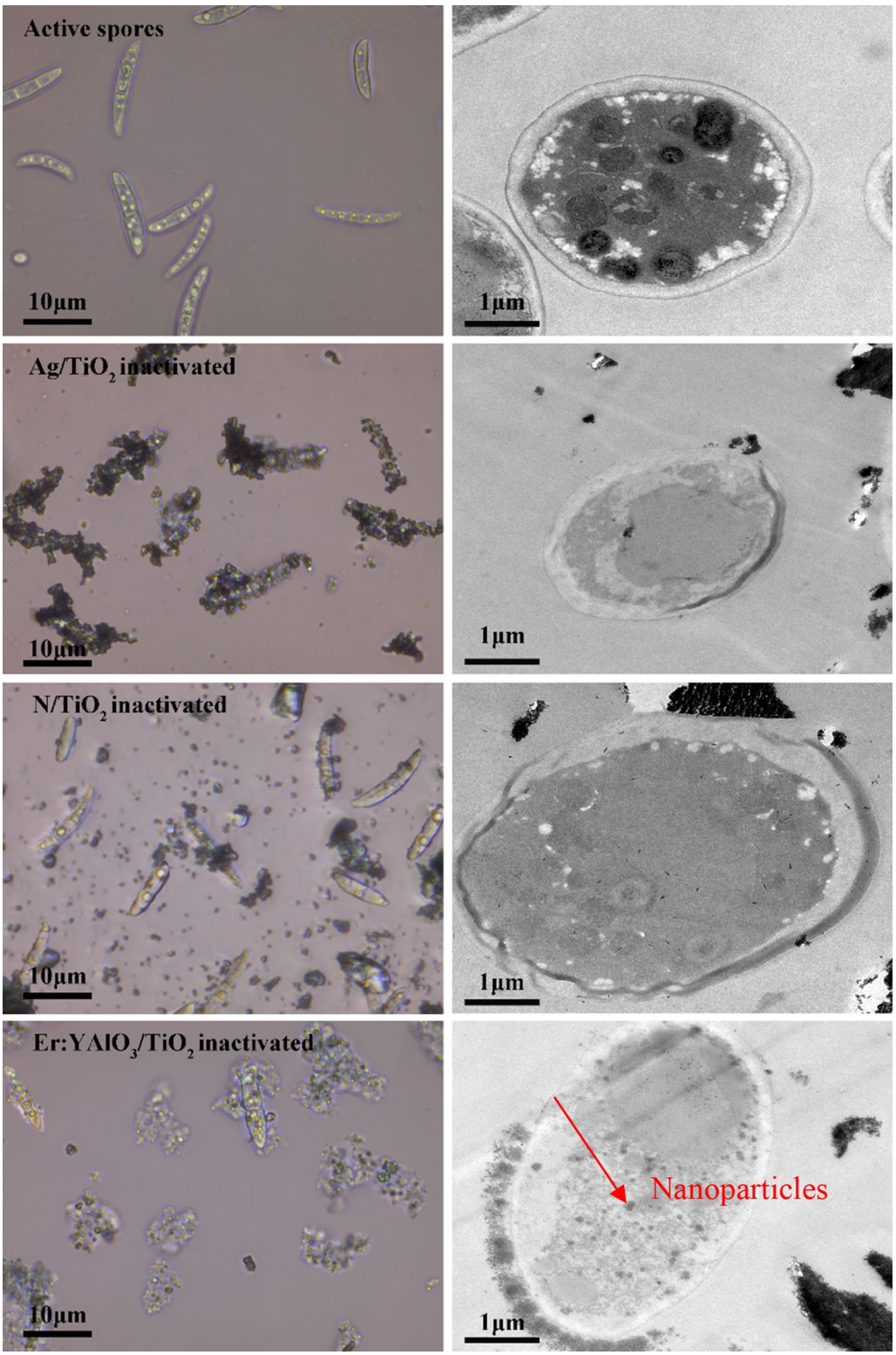

Fig. 3 Optical microscope images (*left column*) and TEM (*right column*) of the active. *F. solani*, and photocatalytically treated *F. solani* with Ag/TiO_2, N/TiO_2 and Er^{3+}:$YAlO_3/TiO_2$, respectively, after 4 h visible light irradiation. The *red arrow* pointed the Er^{3+}:$YAlO_3/TiO_2$ photocatalysis which entered the spores

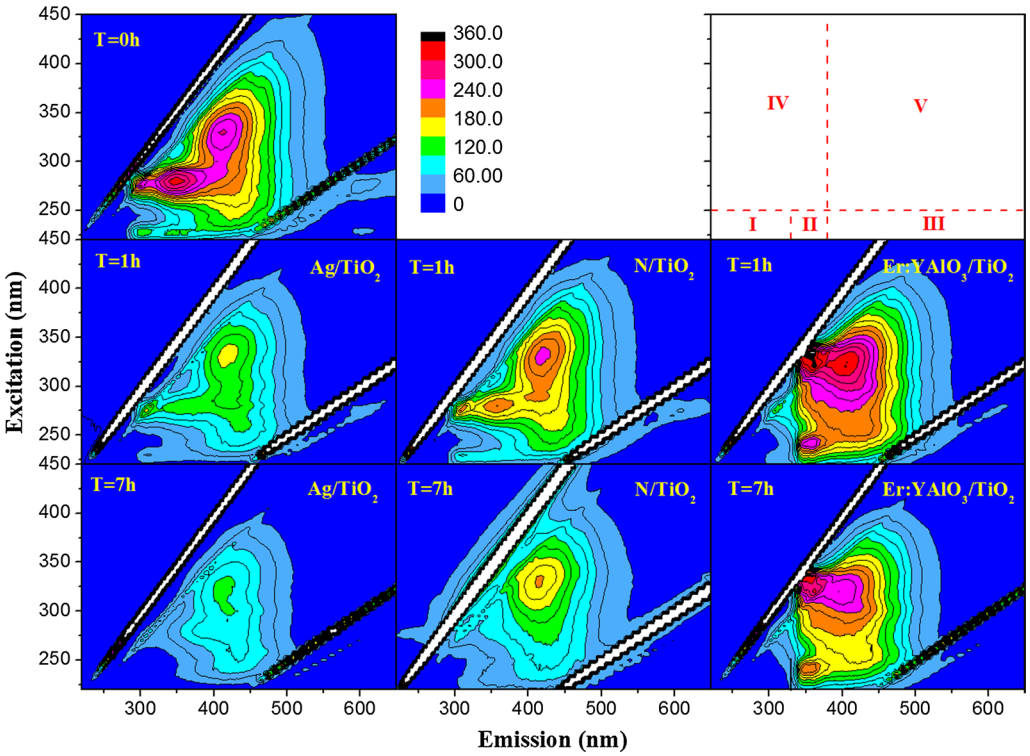

Fig. 4 EEM spectra of the soluble microbial products in the bulk water after *F. solani* inactivation. Five regions were classified, peaks at region I (Ex/Em = 220–250/280–320) are related to tyrosine/tryptophan amino acid; region II is tyrosine/tryptophan protein region with Ex/Em = 220–250/320–380; region III is fulvic acid region with Ex/Em = 220–250/380–460; region IV is soluble microbial byproduct-like material with Ex/Em = 250–380/>280–380 and region V is humic acid-like organics with Ex/Em = 250–380/380–450

degraded the leaked cell contents (confirmed by the TEM results) while inactivating the *F. solani* cells. In the EEM spectra of the Er^{3+}:$YAlO_3$/TiO_2 protocol, the peaks of the tyrosine/tryptophan proteins and soluble microbial byproduct-like compounds were red shifted and enhanced after 1 h, indicating that additional molecules of these species had formed during the inactivation. Moreover, these peaks were only slightly weaker after 7 h treatment, confirming that the new compounds were retained.

The above discussion of the SMP components was supported by the size exclusion chromatography and high performance liquid chromatography (SEC-HPLC) results (see Fig. 5). During 1 h inactivation, the molecular weights (MWs) of the SMPs decreased from 400–1500 kDa to 100–450 kDa in the Ag/TiO_2 treatment and to 340–1200 kDa in the N/TiO_2 treatment. Ag/TiO_2 destroyed the initial cellular macromolecules more extensively than N/TiO_2, and ultimately degraded them to much smaller and presumably less harmful compounds (Ni et al. 2010). After 7 h inactivation, intermediates with MWs as small as 10–70 kDa were detected in the Ag/TiO_2 and N/TiO_2 inactivation protocols, and the intensities of heavier intermediates had significantly decreased. In contrast, the Er^{3+}:$YAlO_3$/TiO_2 protocol slightly increased the MW distribution of the SMPs, from its initial 400–1500 kDa to 600–1600 kDa after 1 h. The increase is attributable to the large MWs of the leaked intercellular material. The intensities of the accumulated SMPs in this MW range increased after 7 h, indicating their harmful and photocatalytically non-degradable characteristics. These high-weight SMPs (400–1600 kDa) are potentially harmful and persistent in the environment (Jarusutthirak and Amy 2007).

Discussion

In this work, *F. solani* spores were inactivated by three prepared photocatalysts, and different inactivation efficiencies, cell damage mechanisms and subsequent SMP leakage levels were observed. The Ag/TiO_2 can kill the spores while maintaining the integrity of their cell walls and simultaneously degrading the SMPs leaked throughout the inactivation. The N/TiO_2 nanoparticles ruptured the cell walls but similarly degraded the leaked SMPs. However, the Er^{3+}:$YAlO_3$/TiO_2 nanoparticles entered the spore cells and significantly oxidized

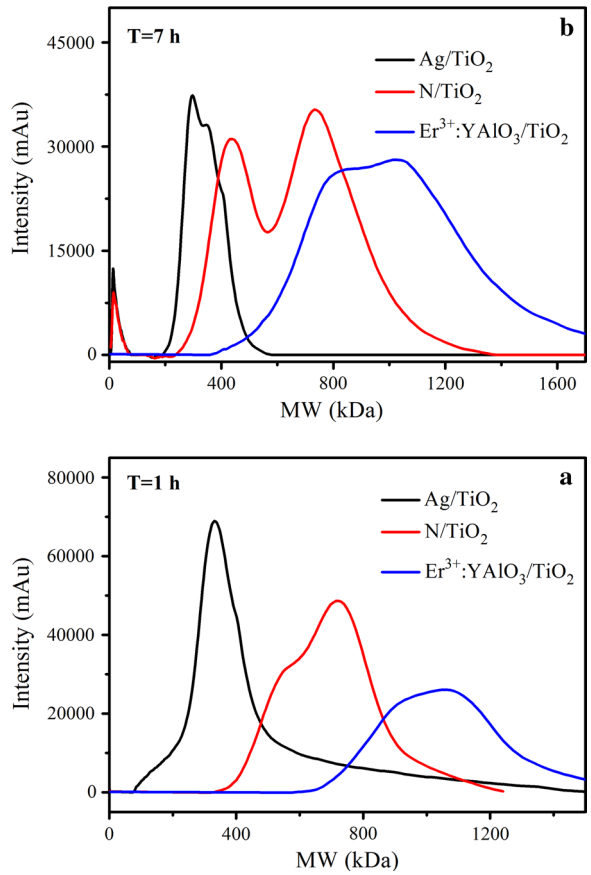

Fig. 5 SEC chromatograms of SMPs during photocatalysis inactivation 1 h (**a**) and 7 h (**b**)

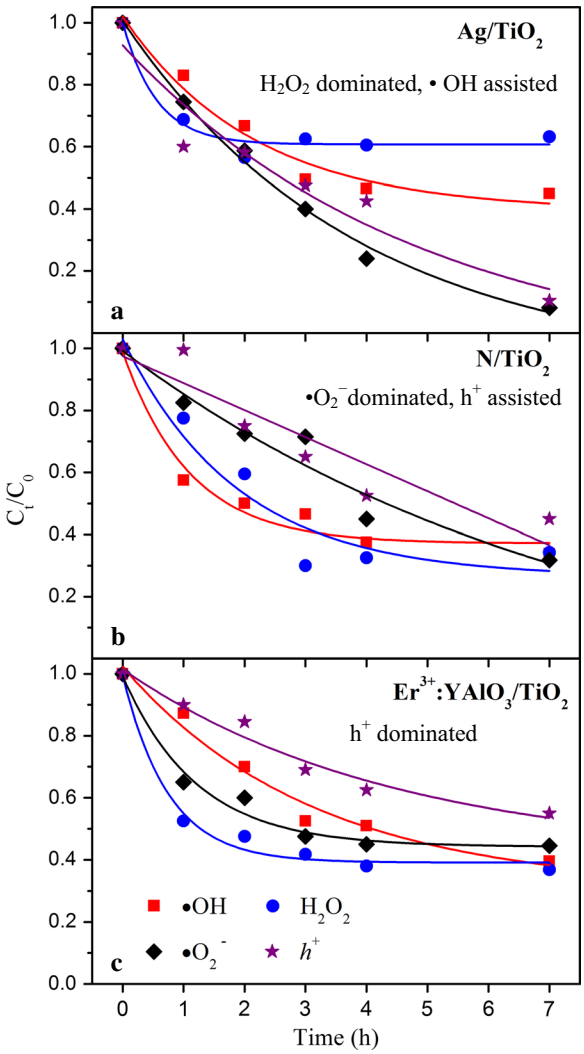

Fig. 6 Inactivation efficiency of *F. solani* by Ag/TiO_2, N/TiO_2 and Er^{3+}:$YAlO_3/TiO_2$ photocatalysts with different scavengers. Legends are the scavenged ROS, and all the values are obtained based on the average of three times experiments

the intercellular contents, which likely explains the large molecular weights of the released SMPs. These differences among the inactivation behaviors were determined by the ROS species generated by the photocatalysts under visible light irradiation (Sun et al. 2014). The photogenerated ROSs, including h^+, •OH, H_2O_2, and $\bullet O_2^-$, are all responsible for bacterial inactivation and play different roles in various photocatalytic systems (Hou et al. 2012).

As shown in Fig. 6, the Ag/TiO_2 photocatalysis system was dominated by H_2O_2 and assisted by •OH. In the N/TiO_2 system, h^+ and $\bullet O_2^-$ played the important roles, with $\bullet O_2^-$ being the most determining species. The Er^{3+}:$YAlO_3/TiO_2$ inactivation system was dominated by h^+. These three ROSs have different average life-spans (4×10^{-9} and 2×10^{-10} s for •OH and $\bullet O_2^-$, respectively, and even shorter for h^+) (Xia et al. 2013). Conversely, H_2O_2 is relatively stable with a half-life of several days in water (Xia et al. 2013). Moreover, in the following generation sequence of ROSs (Chatterjee and Dasgupta 2005), ROSs produced in the earlier steps possess higher oxidizing potential.

$$TiO_2 + h\nu \rightarrow e^- + h^+$$
$$h^+ + H_2O \rightarrow \bullet OH + H^+$$
$$h^+ + OH^- \rightarrow \bullet OH$$
$$O_2 + e^- \rightarrow \bullet O_2^-$$
$$\bullet O_2^- + H^+ \rightarrow HO_2\bullet$$
$$2\,HO_2\bullet \rightarrow O_2 + H_2O_2$$
$$H_2O_2 + O_2^- \rightarrow \bullet OH + OH^- + O_2$$

Thus, the oxidizing potentials of the dominant ROSs generated in this work increased in the order $h^+ > \bullet O_2^- > H_2O_2$.

Accordingly, H_2O_2 has the longest span life but the weakest oxidization capability among the three ROSs.

This species, which dominated the Ag/TiO_2 photocatalysis, diffused into the cells without seriously damaging their cell structures. Consequently, the H_2O_2 molecules permeated the cell membranes, damaging the spores' interiors without excessively leaking their cell contents (as confirmed by the EEM and SEC results). However, the dominant ROS in Er^{3+}:$YAlO_3$/TiO_2 photocatalysis was h^+, with the strongest oxidative potential but shortest life-span among the three ROSs. This species was generally produced on the surface of the catalyst and directly attacked the cell wall. The Er^{3+}:$YAlO_3/TiO_2$ nanoparticles then entered the cells through the broken cell wall, causing abundant leakage of the intracellular components and subsequent pollution of the bulk water quality. The N/TiO_2 photocatalysis was dominated by $\bullet O_2^-$, with a life-span and oxidization capability between those of H_2O_2 and h^+; consequently, the anoxidation performance of this photocatalysis was intermediate between Ag/TiO_2 and Er^{3+}:$YAlO_3/TiO_2$. In summary, the H_2O_2-dominated Ag/TiO_2 photocatalysis delivered outstanding performance in both inactivation efficiency and SMP-leakage control.

Abbreviations

ROSs: reactive oxygen species; *F. solani*: *Fusarium solani*; SMPs: soluble microbial products; XRD: X-ray diffraction; TEM: transmission electron microscopy; EEM: three-dimensional fluorescence spectra; MW: molecular weight; SEC: size exclusion chromatography and; HPLC: high performance liquid chromatography.

Authors' contributions

YD and SD designed the experiments. YD and DM conducted the experiments. YD, HX, ZJ analyzed data. YD wrote the paper with help from DZ. All authors read and approved the final manuscript.

Author details

[1] Key Laboratory of Groundwater Resources and Environment, Ministry of Education, Jilin University, Changchun 130021, Jilin, China. [2] School of Environment, Northeast Normal University, Changchun 130117, China. [3] Jilin Engineering Research Centre for Municipal Wastewater Treatment and Water Quality Protection, Changchun 130117, China.

Acknowledgements

The authors thank the National Natural Science Foundation of China (51578117, 51678279) and Fundamental Research Funds for the Central Universities (2412016KJ011).

Competing interests

The authors declare that they have no competing interests.

Ethical approval and consent to participate

This article does not contain any studies with human participants or animals performed by any of the authors

Funding

This study was funded by the National Natural Science Foundation of China (51578117, 51678270) and the Fundamental Research Funds for the Central Universities (2412016KJ011).

Received: 13 September 2016 Accepted: 24 September 2016
Published online: 01 October 2016

References

Caballero L, Whitehead KA, Allen NS, Verran J (2009) Inactivation of *Escherichia coli* on immobilized TiO_2 using fluorescent light. J Photochem Photobiol A 202:92–98. doi:10.1016/j.jphotochem.2008.11.005

Chatterjee D, Dasgupta S (2005) Visible light induced photocatalytic degradation of organic pollutants. J Photochem Photobiol C: Photochem Rev 6:186–205. doi:10.1016/j.jphotochemrev.2005.09.001

Cho M, Chung HM, Choi WY, Yoon JY (2005) Different inactivation behaviors of MS-2 phage and *Escherichia coli* in TiO_2 photocatalytic disinfection. Appl Environ Microbiol 71:270–275. doi:10.1128/AEM.71.1.270-275.2005

Chong R, Li J, Zhou X, Ma Y, Yang J, Huang L, Han H, Zhang F, Li C (2014) Selective photocatalytic conversion of glycerol to hydroxyacetaldehyde in aqueous solution on facet tuned TiO_2-based catalysts. Chem Commun 50:165–167. doi:10.1039/c3cc46515b

Dong SS, Dong SS, Zhou DD, Zhou X, Ma DM, Du YL (2015) Synthesis of Er^{3+}:Al_2O_3-doped and rutile-dominant TiO_2 composite with increased responsive wavelength range and enhanced photocatalytic performance under visible light irradiation. J Mol Catal A-Chem 407:38–46. doi:10.1016/j.molcata.2015.06.016

Fernández- Ibáñez P, Sichel C, Polo-López MI, Cara-García M, Tello JC (2009) Photocatalytic disinfection of natural well water contaminated by *Fusarium solani* using TiO_2 slurry in solar CPC photo-reactors. Catal Today 144:62–68. doi:10.1016/j.cattod.2009.01.039

Fernández-Ibáñez P, Polo-López MI, Malato S, Wadhwa S, Hamilton JWJ, Dunlop PSM, D'Sa R, Magee E, O'Shea K, Dionysiou DD, Byrne JA (2015) Solar photocatalytic disinfection of water using titanium dioxide grapheme composites. Chem Eng J 261:36–44. doi:10.1016/j.cej.2014.06.089

Foster HA, Ditta IB, Varghese S, Steele A (2011) Photocatalytic disinfection using titanium dioxide: spectrum and mechanism of antimicrobial activity. Appl Microbiol Biotechnol 90:1847–1868. doi:10.1007/s00253-011-3213-7

Hou Y, Li XY, Zhao QD, Chen GH, Raston CL (2012) Role of hydroxyl radicals and mechanism of *Escherichia coli* inactivation on $Ag/AgBr/TiO_2$ nanotube array electrode under visible light irradiation. Environ Sci Technol 46:4042–4050. doi:10.1021/es204079d

Jarusutthirak C, Amy G (2007) Understanding soluble microbial products (SMP) as a component of effluent organic matter (EfOM). Wat Res 41:2787–2793. doi:10.1016/j.watres.2007.03.005

Kikuchi Y, Sunada K, Iyoda T, Hashimoto K, Fujishima A (1997) Photocatalytic bactericidal effect of TiO_2 thin films: dynamic view of the active oxygen species responsible for the effect. J Photochem Photobiol 106:51–56. doi:10.1016/S1010-6030(97)00038-5

Kontos AI, Kontos AG, Raptis YS, Falaras P (2008) Nitrogen modified nanostructured titania: electronic, structural and visible-light photocatalytic properties. Phys Status solidi-R 2:83–85. doi:10.1002/pssr.200802006

Lee MS, Hong SS, Mohseni M (2005) Synthesis of photocatalytic nanosized TiO_2–Ag particles with sol–gel method using reduction agent. J of Mol Catal A-Chem 242:135–140. doi:10.1016/j.molcata.2005.07.038

Lu D, Zhang M, Zhang Z, Li Q, Wang X, Yang J (2014) Self-organized vanadium and nitrogen co-doped titania nanotube arrays with enhanced photocatalytic reduction of CO_2 into CH_4. Nanoscale Res Lett 9:272. doi:10.1021/acs.est.5b00989

Nakamura R, Tanaka T, Nakato Y (2004) Mechanism for visible light responses in anodic photocurrents at N-doped TiO_2 film electrodes. J Phys Chem B 108:10617–10620. doi:10.1021/jp048112q

Ni BJ, Zeng RJ, Fang F, Xie WM, Sheng GP, Yu HQ (2010) Fractionating soluble microbial products in the activated sludge process. Wat Res 44:2292–2302. doi:10.1016/j.watres.2009.12.025

Polo-López MI, Fernández- Ibáñez P, García-Fernández I, Oller I, Salgado-Tránsito I, Sichel C (2010) Resistance of *Fusarium*sp spores to solar TiO_2 photocatalysis: influence of spore type and water scaling-up results. J Chem Technol Biotechnol 85:1038–1048. doi:10.1002/jctb.2397

Polo-López MI, Castro-Alférez M, Oller I, Fernández-Ibáñez P (2014) Assessment of solar photo-Fenton, photocatalysis, and H_2O_2 for removal of phytopathogen fungi spores in synthetic and real effluents of urban wastewater. Chem Eng J 257:122–130. doi:10.1016/j.cej.2014.07.016

Rahmanto AS, Pattison DI, Davies MJ (2005) Photo-oxidation-induced inactivation of the selenium-containing protective enzymes thioredoxin reductase and glutathione peroxidase. Free Radical Bio Med 53:1308–1316. doi:10.1016/j.freeradbiomed.2012.07.016

Shah SI, Li W, Huang CP, Jung O, Ni C (2002) Study of Nd^{3+}, Pd^{2+}, Pt^{4+}, and Fe^{3+} dopant effect on photoreactivity of TiO_2 nanoparticles. PNAS 99:6482–6486. doi:10.1073/pnas.052518299

Spurr RA, Myers H (1957) Quantitative analysis of anatase-rutile mixtures with an X-ray diffractometer. Anal Chem 29(5):760–762. doi:10.1021/ac60125a006

Sun HW, Li GY, Nie X, Shi HX, Wong PK, Zhao HJ, An TC (2014) Systematic approach to in-depth understanding of photoelectrocatalytic bacterial inactivation mechanisms by tracking the decomposed building blocks. Environ Sci Technol 48:9412–9419. doi:10.1021/es502471h

Thabet S, Weiss-Gayet M, Dappozze F, Cotton P, Guillard C (2013) Photocatalysis on yeast cells: toward targets and mechanisms. Appl Catal B-Environ 140–141:169–178. doi:10.1016/j.apcatb.2013.03.037

Thabet S, Simonet F, Lemaire M, Guillard C, Cotton P (2014) Impact of photocatalysis on fungal cells: depiction of cellular and molecular effects on *saccharomyces cerevisiae*. Appl Environ Microb 80:7527–7535. doi:10.1128/AEM.02416-14

Turki A, Kochkar H, García-Fernández I, Polo-López MI, Ghorbel A, Guillard C, Berhault G, Fernández-Ibáñez P (2013) Solar photocatalytic inactivation of *Fusarium Solani* over TiO_2 nanomaterials with controlled morphology—formic acid effect. Catal Today 209:147–152. doi:10.1016/j.cattod.2012.10.014

Wang J, Xie YP, Zhang ZH, Li J, Li CW, Zhang LQ, Xing ZQ, Xu R, Zhang XD (2010) Photocatalytic degradation of organic dyes by Er^{3+}:$YAlO_3$/TiO_2 composite under solar light. Environ Chem Lett 8:87–93. doi:10.1016/j.solmat.2010.03.003

Xia D, Ng TW, An T, Li G, Li Y, Yip HY, Zhao H, Lu A, Wong PK (2013) A recyclable mineral catalyst for visible-light-driven photocatalytic inactivation of bacteria: natural magnetic sphalerite. Environ Sci Technol 47:11166–11173. doi:10.1021/es402170b

Xie WM, Ni BJ, Seviour T, Sheng GP, Yu HQ (2012) Characterization of autotrophic and heterotrophic soluble microbial product (SMP) fractions from activated sludge. Wat Res 46:6210–6217. doi:10.1016/j.watres.2012.02.046

Zhou DD, Xu ZX, Dong SS, Huo MX, Dong SS, Tian XD, Cui B, Xiong HF, Li TT, Ma DM (2015) Intimate coupling of photocatalysis and biodegradation for degrading phenol using different light types: visible light vs UV light. Environ Sci Technol 49:7776–7783. doi:10.1021/acs.est.5b00989

Zuo F, Bozhilov K, Dillon RJ, Wang L, Smith P, Zhao X, Bardeen C, Feng P (2012) Active facets on titanium (III)-doped TiO_2: an effective strategy to improve the visible-light photocatalytic activity. Angew Chem 124:6327–6330. doi:10.1002/ange.201202191